DNS of Surface Textures to Control the Growth of Turbulent Spots

James S. Strand[1] and David B. Goldstein[2]
The University of Texas at Austin, Austin, TX, 78712

A spectral DNS code was used to study the growth and spreading of turbulent spots in a nominally laminar, zero-pressure gradient boundary layer. In addition to the flat wall case, the interaction of these spots with passive surface textures (riblets and fins) was examined. The dimensions of these textures were chosen based on parametric studies performed in past work, with the goal of achieving maximum reduction of spot spreading. The flat plate, surface textures, and initial spot perturbation were simulated via an immersed boundary method, and a "suction-wall" allowed the available channel code to model a boundary layer. In all cases, self-similar arrowhead shaped spots formed. The swirling strength was used to visualize the vortical structures within a spot, and a developed spot was found to consist primarily of a multitude of hairpin vortices. The riblets and the fins both decreased the average spot spreading rate by 7-8% from the flat wall value.

Nomenclature

U_∞ = free-stream velocity
u = streamwise velocity
v = wall-normal (vertical) velocity
w = spanwise velocity
δ_o^* = boundary layer displacement thickness at the location of the perturbation
δ_o = boundary layer 99% thickness at the location of the perturbation
ν = kinematic viscosity
h = surface texture height
s = surface texture crest-to-crest spacing
t = time
x = streamwise coordinate
y = wall-normal coordinate
z = spanwise coordinate
L = streamwise length of the computational domain
W = spanwise width of the computational domain

I. Introduction

Turbulent Spots

Turbulent spots form naturally during the boundary layer transition process. These spots take on an arrowhead shape, pointing downstream. The spots appear at randomly distributed points and their growth and merging lead to complete transition to turbulence. A spot appears as a fairly well defined region of turbulence surrounded by laminar flow.

Turbulent spots can also be artificially generated with a localized perturbation in a laminar boundary layer. Wygnanski et al.[1] studied artificially generated spots in detail. Amini and Lespinard[2] introduced a perturbation by injecting fluid through a hole in the flat plate by means of a loudspeaker. They were primarily interested in studying a pre-turbulent spot, but their method of perturbation did generate the same arrowhead-shaped turbulent spots as did other experiments. Using isodeviation contours of mean velocity, they estimated the spreading angle of the turbulent spot to be ~10°, and the apex angle to be ~30°. For a schematic of a turbulent spot, with spreading angle, apex angle, etc. labeled, see Fig. 1.

[1] Graduate Researcher, Aerospace Engineering Dept., 1 University Station, C0600, Student Member.
[2] Professor, Aerospace Engineering Dept., 1 University Station, C0600, Senior Member.

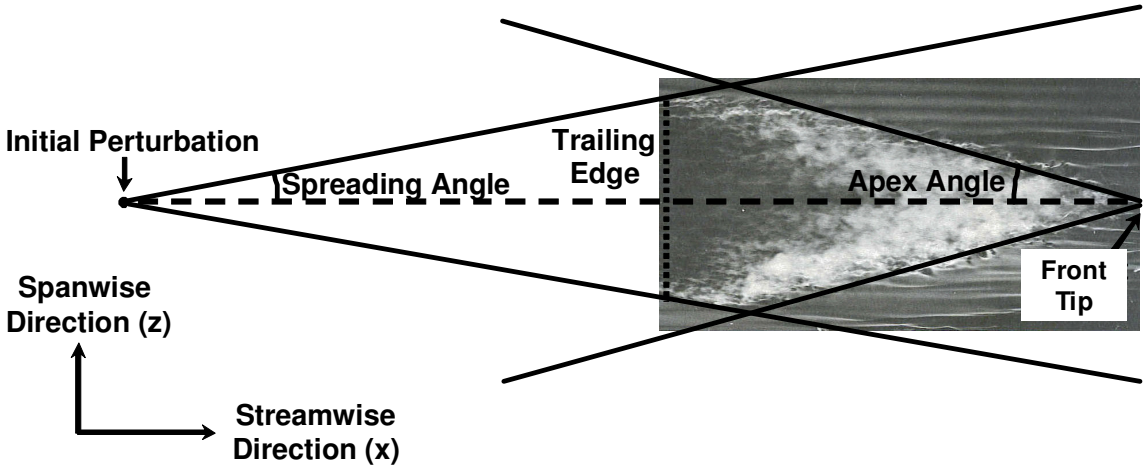

Figure 1: Schematic top view of a turbulent spot. The spot photograph used here was taken by R. E. Falco using smoke in a wind tunnel flow over a flat plate at Re_x = 400,000, and was found in *An Album of Fluid Motion*, by Milton Van Dyke (1982).

DNS has also been used to simulate turbulent spots. Henningson et al.[3] used a spectral method to simulate the growth and spreading of a turbulent spot in an incompressible flat plate boundary layer. The domain for these simulations was periodic in the streamwise and spanwise directions. To approximate the effect of the thickening of the surrounding boundary layer as the spot moves downstream, a weak body force was applied. The perturbation used to induce the spot was a localized, impulsive body force directed upstream. The spots exhibited self-similar growth, as found by experiments. Henningson et al. state that "The turbulent vortical region grows at a half-angle of about 7°. The region in which the velocity is disturbed is wider, about 10°, in good agreement with experimental results." It was found that the growth of the spot became self-similar after $tU_\infty/\delta_o \approx 100$. The trailing edge of the spot moved at ~$0.5U_\infty$, and the leading edge at ~$0.83U_\infty$, and Henningson et al. note that these values compare reasonably well with the commonly quoted experimental values of $0.5U_\infty$ and $0.9U_\infty$, respectively. They also observed an overhang region at the leading edge of the spot, which is consistent with the experiments of Wygnanski et al.[1]

Singer and Joslin[4] focused their DNS simulations on the development of a turbulent spot in an incompressible, laminar, zero-pressure-gradient boundary layer. Their domain was periodic in the spanwise direction, and they used a buffer-domain in the streamwise direction to allow for a non-reflective boundary condition on the streamwise velocity. Fluid injection through a short streamwise slot was used to perturb the flow and generate the disturbance that grew into the turbulent spot. Singer[5] used the same code and method to further simulate the growth of the young turbulent spot. The simulated spot shared many characteristics with experimentally observed spots (such as those described by Wygnanski et al.[1]), including a distinct overhang region and a calm but non-Blasius region in the wake of the spot. The spanwise-averaged skin friction coefficient varies widely along the spot centerline, but when this value is averaged over the length of the spot region, the average value is closer to the turbulent value than the laminar one. A spatially averaged velocity profile does not show a distinct logarithmic region, but Singer states that the flow is likely beginning to develop a log layer. He calculates a trailing edge speed of $0.63U_\infty$ and a leading edge speed of $0.94U_\infty$. For the spreading angle, he reports values of 3.8° or 6.4°, depending on whether the origin for the spreading is defined as before or after a particularly large discontinuity in the plot of the spanwise extent of the spot versus the streamwise location of the spanwise edge. Although these values are significantly lower than previously reported experimental values, he argues that this is probably due to the fact that the Reynolds number (based on distance from the perturbation to the measurement location) was about 80,000, which is significantly lower in the simulation than in most experiments (Wygnanski et al.[1] took some data at Re_x = 120000, but most of their results were for Re_x = 600000).

Recent work by Jocksch and Kleiser[13] examined the development of turbulent spots in a simulated supersonic flat plate boundary layer. Their spots exhibited the familiar properties of incompressible spots (arrowhead shape, overhang region at the front, etc.). Making use of the swirling strength, they identified multiple hairpin vortices within their spots.

Constraining Spot Growth and Spreading

We have shown previously[6,11] that properly dimensioned surface textures can reduce the spreading angle of turbulent spots by 10-20%. In that prior work a small parametric study was performed to examine the effects of different texture dimensions. In this work we have used only three geometries: the best case riblets and best case fins (those that reduced spot spreading the most in the prior work), and the flat wall. The spots in the prior work were followed for a distance of ~450 δ_o^*, and at the end of the domain Re_x was ~200,000. In this work, a larger domain allowed us to follow spots over a greater distance, in order to determine whether the previously observed reductions in spreading angle are maintained at higher Re_x and further downstream of the initial perturbation. With $Re_x \approx 300{,}000$ at the end of the domain, we are closer to the Reynolds numbers used in past experiments, such as those of Wygnanski et al.[1] mentioned earlier. This allows for better comparison between our results and those of the experiments. Following the spot further also gives us more accuracy in calculating the spreading rate, and allows us to determine with more certainty the extent to which the spreading is decreased by the textures.

II. Numerical Method

There exist several approaches to simulating laminar and turbulent boundary layers over textured surfaces. Goldstein et al.[7] combined the spectral code described by Handler et al.[8] (which is based on the spectral method of Kim et al.[9]) with an immersed boundary technique, to allow for the simulation of laminar or turbulent flows over a multitude of stationary or moving solid surfaces. This technique for modeling an immersed boundary introduces a localized body force field into the Navier Stokes equations. The force field is made to adapt to the flow and bring it to a specified velocity on the immersed boundary points. This adaptation takes place by means of a two-parameter control scheme, which provides feedback based on both the current velocity at the point, and the prior history of the velocity at that point (an integral term). The vector equation for the control scheme is

$$\mathbf{F}(\mathbf{x},t) = \alpha \int_0^t \left[\mathbf{U}(\mathbf{x},t') - \mathbf{U}_{\mathbf{des}}(\mathbf{x},t')\right] dt' + \beta\left[\mathbf{U}(\mathbf{x},t) - \mathbf{U}_{\mathbf{des}}(\mathbf{x},t)\right] \qquad (1)$$

where $\mathbf{U}(\mathbf{x},t)$ is the actual velocity vector at a given grid point which forms part of the immersed boundary, $\mathbf{U}_{\mathbf{des}}(\mathbf{x},t)$ is the desired velocity vector at that point, α and β are negative constants, and $\mathbf{F}(\mathbf{x},t)$ is the body force vector which is applied in the region of that grid point. The gain parameters α and β are generally constant in time, but they may be functions of position. This same base control scheme can be used for other purposes besides creating solid or moving surfaces, as discussed later in this section. For a more detailed explanation of the immersed boundary method employed here, see Goldstein et al.[7]

The code described above was originally designed for channel flow, and some modifications were required to allow the simulation of a boundary layer. First, a buffer zone was added to create the desired inlet Blasius profile. The buffer zone uses the same control scheme as the solid immersed boundaries, but with parameters that are spatially dependent. See Goldstein et al.[10] for a more detailed description of the buffer zone.

If no further modifications are made to the original channel-flow code, a favorable pressure gradient develops in the streamwise direction and the boundary layer does not grow downstream as the Blasius solution predicts. This happens because even when the top wall of the channel is set to allow slip, it still permits no through flow. There is always some small but finite vertical velocity above a flat plate in an infinite domain, even very far from the plate. Thus in order to model the boundary layer, it is necessary to accommodate this vertical velocity. The top wall of the channel cannot be modified to allow through flow, so a different type of immersed boundary was placed below the top channel wall to force a suitable upflow. The vertical velocity at all points on this "suction wall" is forced (by the control scheme described earlier) to be that predicted by the Blasius solution, thus allowing normal streamwise growth of the boundary layer. Unlike the solid-wall immersed boundaries, the suction wall only applies the body force in the vertical direction; it exerts no force in the spanwise or streamwise directions. This suction wall serves the same purpose as a small variation in area in a real wind tunnel, which is used to maintain a zero pressure gradient in a test section. The boundary layer can be made to grow as if from the leading edge of the plate (the plate starts at or near the end of the buffer zone) or the velocity can be set in the buffer zone to a Blasius profile for a given x-location on the plate. In either case the profile will develop correctly downstream.

A schematic diagram in Figure 2 shows the locations of the buffer zone, the suction wall, and the flat plate virtual surface. In the top image the y-direction is exaggerated by ten times compared to the x-direction, but with this scaling in mind, the dimensions are otherwise correct. See Strand[6] for a detailed discussion of the locations, purposes, and interactions of the various immersed boundaries in the domain.

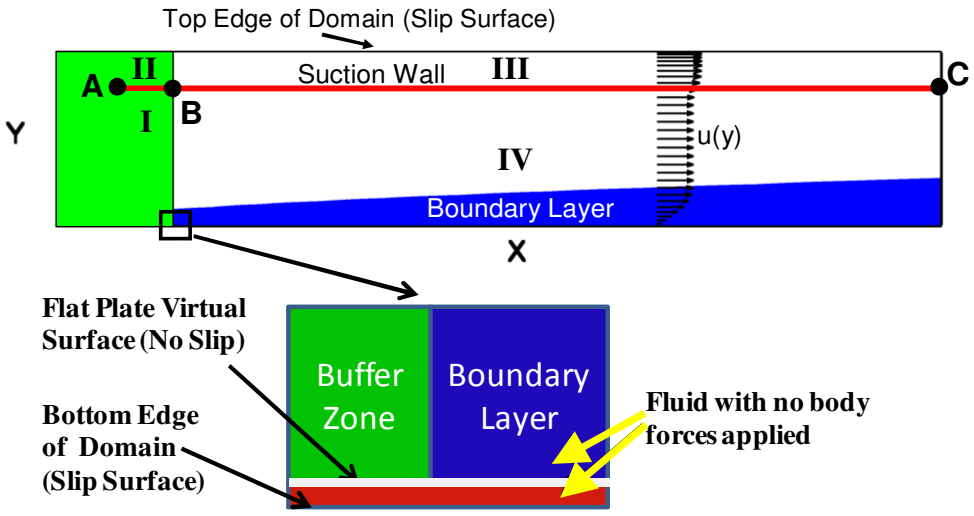

Figure 2: Schematic of computational domain with buffer zone and suction wall employed to model a Blasius boundary layer. Top image shows entire domain, and is stretched in the y-direction but is otherwise to scale. Bottom image shows the virtual flat plate, and the small area of fluid beneath it. Region IV is the region of interest in which the spots develop.

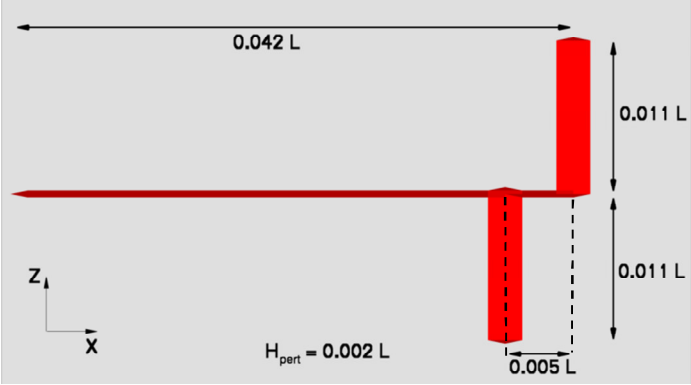

Figure 3: Top view of the perturbation shape used to generate the turbulent spots. Perturbation extends upward from the flat plate. H_{pert} is the perturbation height and L is the length of the domain in the streamwise direction.

The perturbation used to generate the turbulent spot is a solid surface, created with the immersed boundary method, which is introduced into the flow briefly at the beginning of the simulation and then removed. Figure 3 gives the shape and dimensions of the perturbation. The perturbation used in this work differs from that used in our prior work[6,11] where a smooth, flattened hemisphere was used. Since the immersed boundary forces are applied at the grid nodes, any "smooth" surface will actually be stairstepped, and thus the shape of the flattened hemisphere perturbation changed slightly when the grid resolution changed. The current perturbation has a shape which remains constant regardless of grid resolution. The perturbation is asymmetric about the spanwise centerline in order to force asymmetry in the turbulent spot, since experimental spots do not have perfect left/right symmetry.

As stated earlier, spots were examined over three surfaces: a flat wall, riblets, and fins. The riblets and fins are solid, no-slip surfaces created with the immersed boundary method. The riblets and fins both have the same crest-to-crest spacing of 1.1 δ_o^*, where δ_o^* is the boundary layer displacement thickness at the location of the perturbation, as calculated from the Blasius solution. The height of the riblets is 1.1 δ_o^* (21 grid points) and the height of the fins is 0.8 δ_o^* (18 grid points). The grid points are not equally spaced in the wall normal direction, rather they follow a cosine grid, and are most closely spaced at the wall. In both cases, the total number of individual textures is 144. The textures are composed of 8 grid points in the spanwise direction (in the case of the riblets these points define the slope of the riblet sides, in the case of the fins there are 7 grid points of flat wall between the fins, which are only one grid point wide).

The textures do not begin immediately downstream of the buffer zone, instead they begin at 0.208 L, and ramp up over a distance of 0.042 L (where L is the total length of the domain in the streamwise direction. For reference, the buffer zone ends at 0.083 L.) Figure 4 is a schematic for the riblet case, and Figure 5 is a similar schematic for the fin case. So that they can easily be seen, the riblets and fins used in these two schematics have heights and spacings significantly larger than those of the textures used in the actual runs. Only the part of the domain near the bottom wall is shown; the suction wall is located well above the visible area.

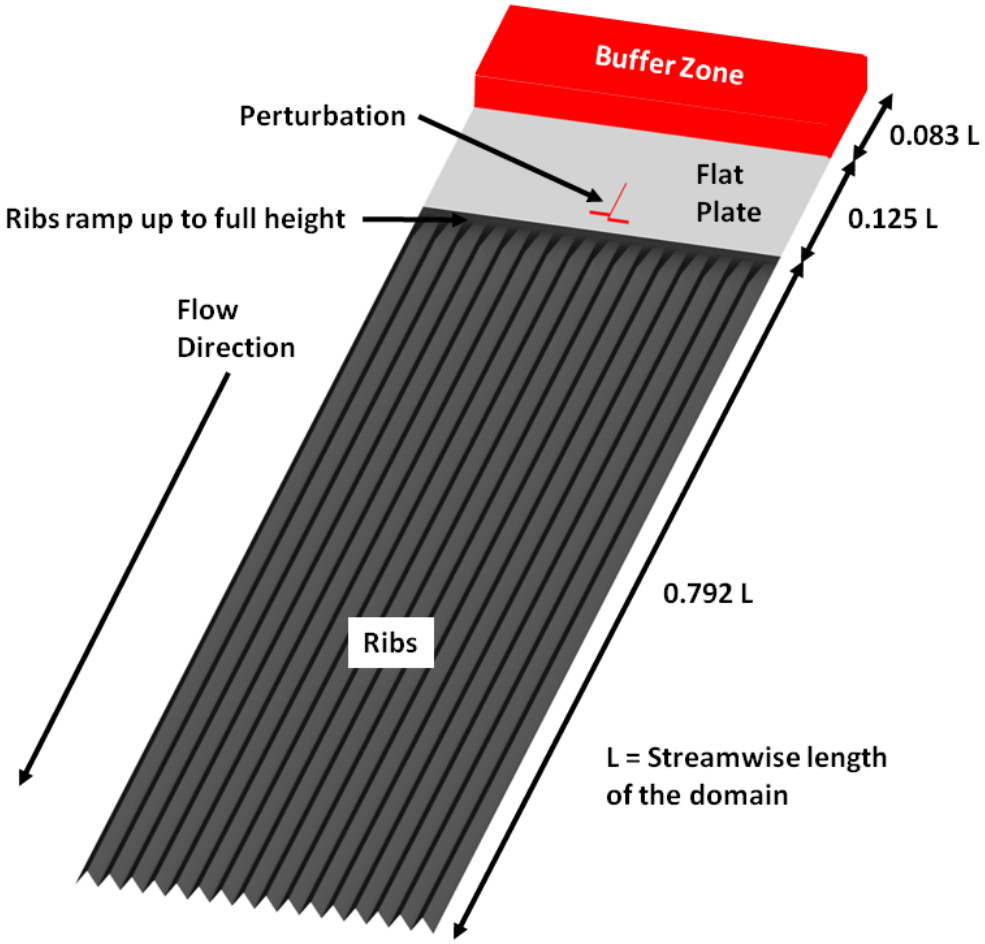

Figure 4: Schematic for riblet case showing 16 riblets, the perturbation, and the buffer zone.

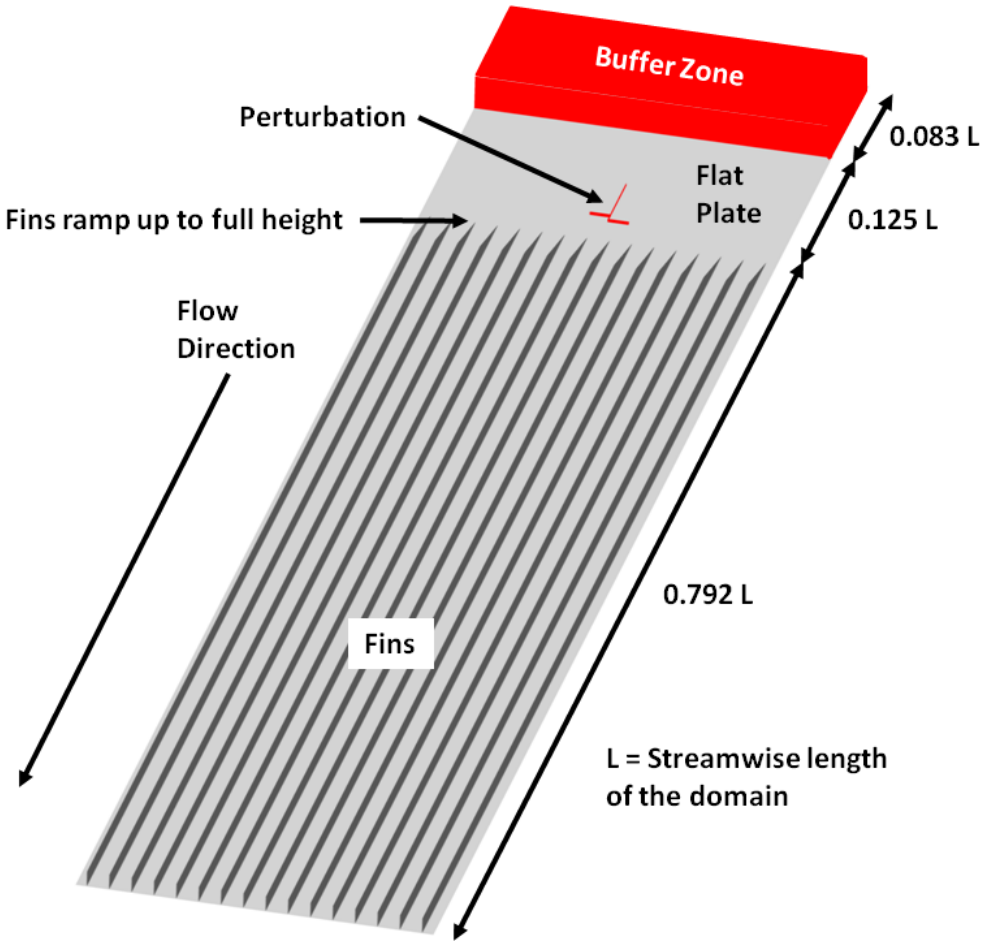

Figure 5: Schematic for the fin case showing 16 fins, the perturbation, and the buffer zone.

III. Results and Discussion

Spot Structure

Before the effects of surface textures on spots are investigated it is useful to examine spots over a flat plate. This provides a basis for comparison both with the surface texture runs presented later and with the experiments, simulations, and flow visualization found in the literature.

The domain used for these simulations had dimensions of 796.1 δ_o^*, 31.8 δ_o^*, and 159.2 δ_o^* in the streamwise (x), wall-normal (y), and spanwise (z) directions, respectively. For this domain, 768×192×768 spectral modes were used in the x, y, and z directions, respectively. The perturbation was introduced at t = 0 and remained in the flow until t = 4.8 δ_o^*/U_∞. The simulation continued until t = 859.8 δ_o^*/U_∞, by which time the front tip of the spot had reached the end of the streamwise domain. The Reynolds number based on displacement thickness, Re_{δ^*}, was 376.8 at the perturbation location. Re_x at the end of the streamwise domain was 298000 (for comparison, Wygnanski et al.[1] took some data at Re_x = 120000, but most of their results were for Re_x = 600000, as mentioned earlier).

A top-down view of the flat-wall spot at three different simulation times is shown in Fig. 6. The time interval between t_1 and t_2 is the same as that between t_2 and t_3. As the spot matures, it takes on the expected arrowhead shape. It is asymmetric about the spanwise centerline since the perturbation itself is asymmetric. A quick glance at the figure indicates that the leading edge is moving at a fairly constant speed, since the leading edge moves about the same distance between t_1 and t_2 as it does between t_2 and t_3.

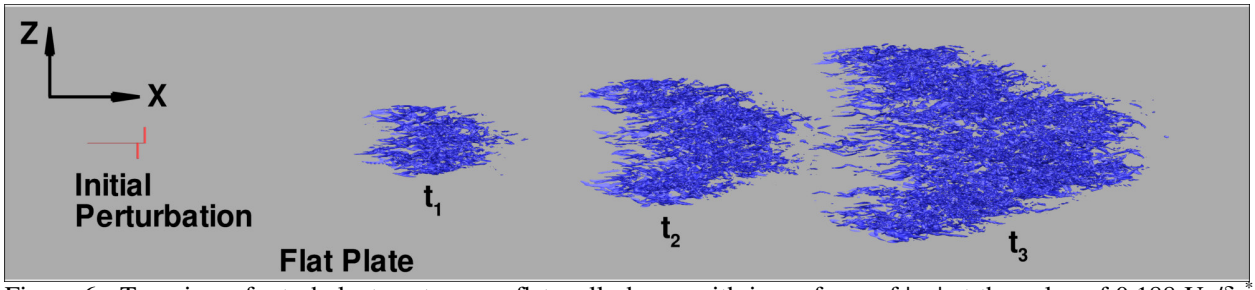

Figure 6: Top view of a turbulent spot over a flat wall, drawn with isosurfaces of $|\omega_x|$ at the value of 0.188 U_∞/δ_o^* and shown at $t_1 = 286.6\ \delta_o^*/U_\infty$, $t_2 = 525.4\ \delta_o^*/U_\infty$, and $t_3 = 764.2\ \delta_o^*/U_\infty$.

Figure 7 shows a close-up side view of the flat wall spot. The overhang found by prior experiments and DNS simulations is clearly visible near the leading edge of the spot.

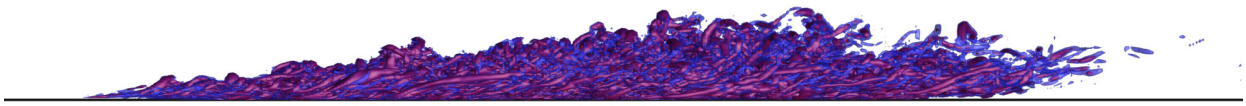

Figure 7: Side view of the flat wall spot at time $t = 740.4\ \delta_o^*/U_\infty$ shown with two isosurfaces of λ_2. Blue isosurfaces are at a value of $-0.0044\ (U_\infty/\delta_o^*)^2$ and are semi-translucent, red isosurfaces are at a value of $-0.0089\ (U_\infty/\delta_o^*)^2$.

Figures 8-10 are oblique perspective views from the rear of the flat wall spot. Two isosurfaces of the swirling strength, λ_2, are present in each figure, one at the value of $-0.0089\ (U_\infty/\delta_o^*)^2$ and the other at $-0.0044\ (U_\infty/\delta_o^*)^2$, and translucency is used so that both isosurfaces can be seen. The usefulness of the swirling strength is apparent here; these isosurfaces of λ_2 clearly display the multiple overlapping and entwined hairpin and streamwise vortical structures that make up the growing spot. Hairpins are present throughout the spot. The structures are more complex and intertwined in the spot center, and the hairpin legs do not necessarily align fully with the streamwise direction. The hairpins present in the first image (Fig. 8) are almost all of roughly the same size. As the spot matures the range of hairpin sizes increases, and in the last image (Fig. 10) a wide variety of hairpin scales is apparent. In these figures the relaminarization of the flow after the passage of the spot is apparent, since there are no vortical structures present in the wake of the spot.

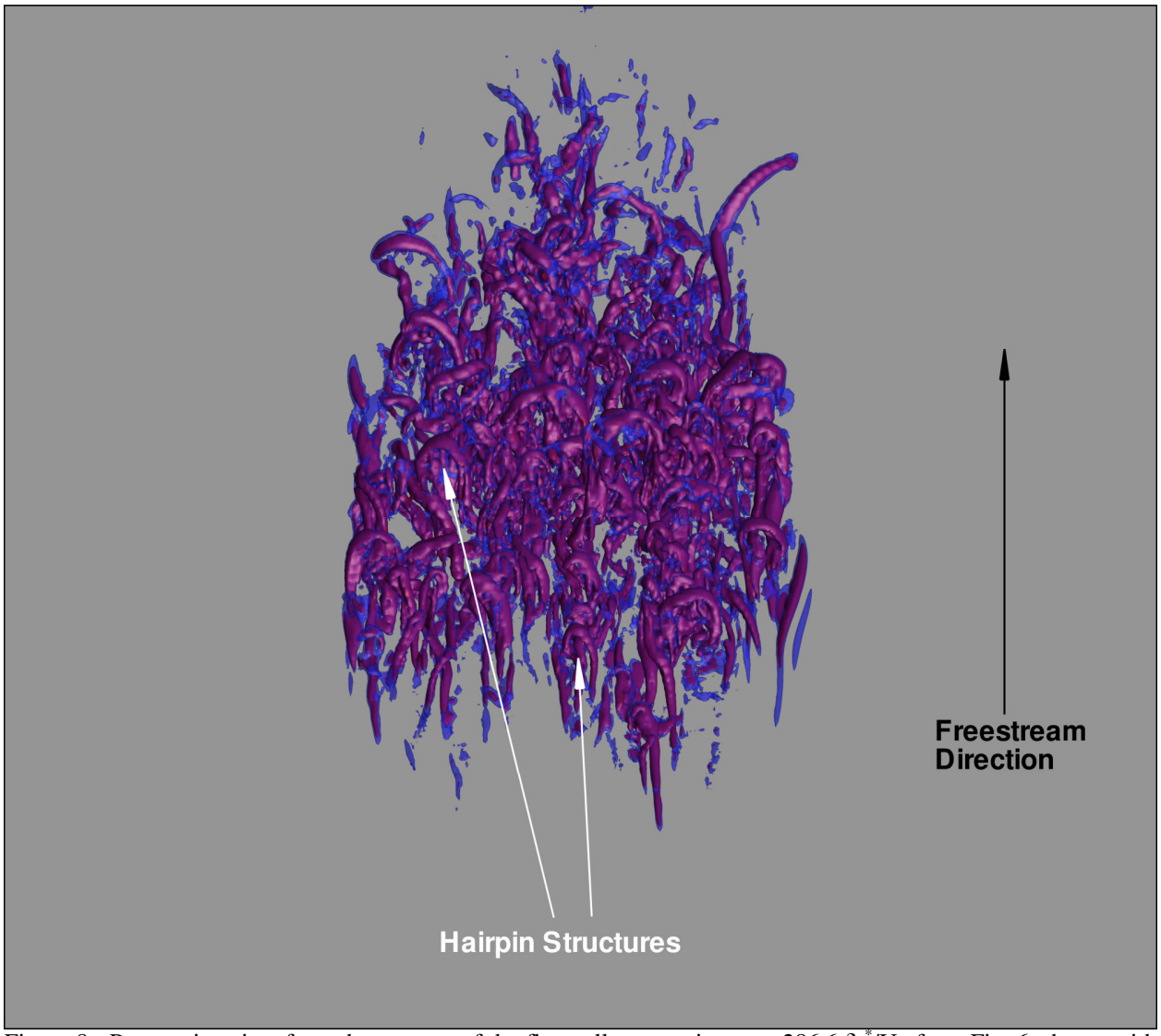

Figure 8: Perspective view from the top rear of the flat wall spot at time $t_1 = 286.6\ \delta_o^*/U_\infty$ from Fig. 6, shown with two isosurfaces of λ_2. Blue isosurfaces are at a value of -0.0044 $(U_\infty/\delta_o^*)^2$ and are semi-translucent, red isosurfaces are at a value of -0.0089 $(U_\infty/\delta_o^*)^2$. Viewer is 40° above the horizontal looking down toward the spot and facing downstream. Hairpins all appear to be of roughly the same size.

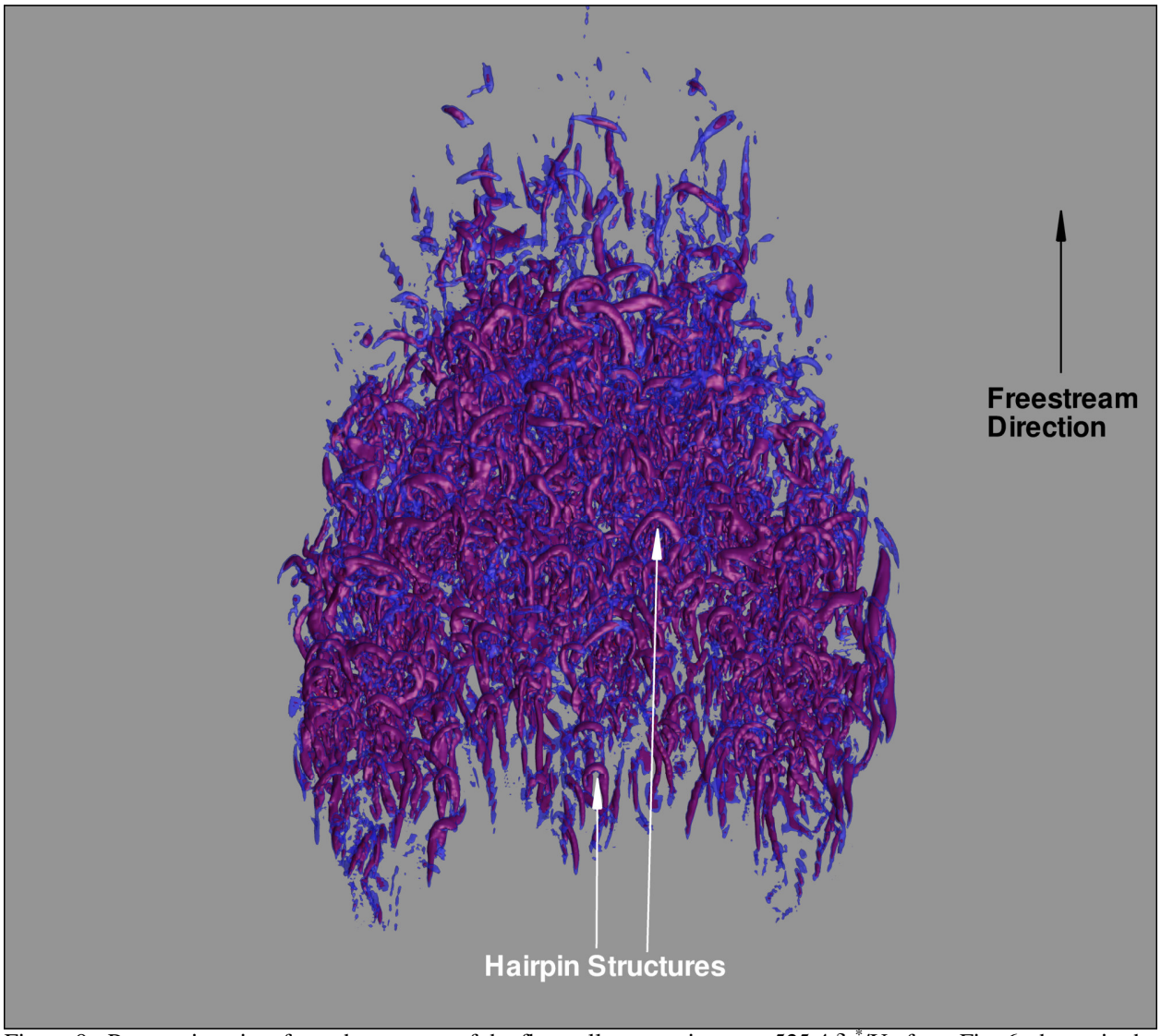

Figure 9: Perspective view from the top rear of the flat wall spot at time $t_2 = 525.4\ \delta_o^*/U_\infty$ from Fig. 6, shown in the same way as the spot in Fig. 8. The range of hairpin sizes appears to be increasing.

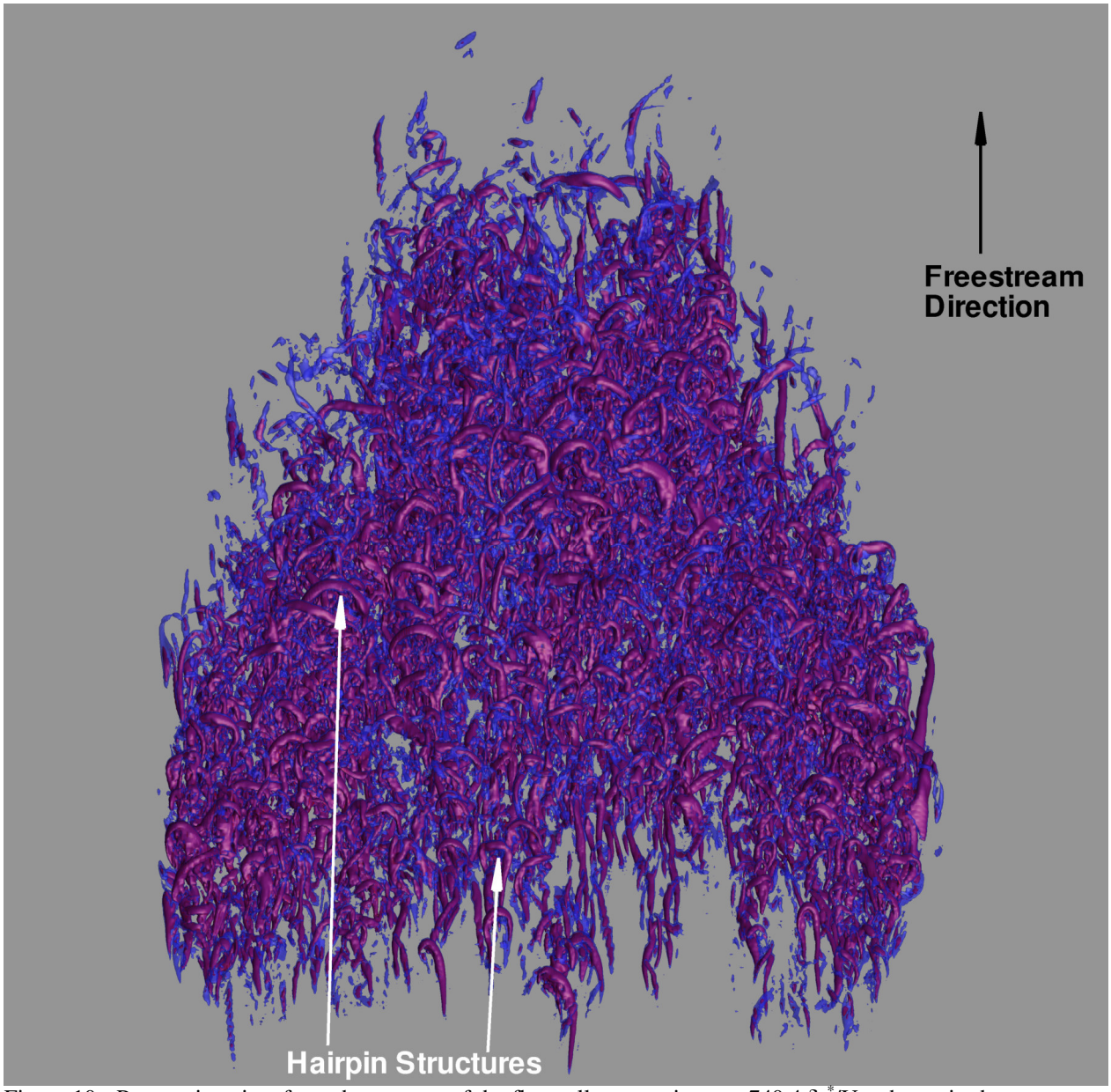

Figure 10: Perspective view from the top rear of the flat wall spot at time t = 740.4 δ_o^*/U_∞, shown in the same way as the spot in Fig. 8. A variety of hairpin scales are apparent.

The bulk of the work presented here concerns surface textures and their ability to constrain spot spreading. This will be discussed more in the next section, but some qualitative results are presented here for the surface texture cases. To this end, Figure 11 shows zoomed in views of the top of the spot for the flat wall, riblet, and fin cases. There is not a great deal of qualitative difference between the spots. All three have the same intertwined hairpin structures, and roughly the same density of vortical structures inside the spot (none of the cases has clearly weaker or stronger turbulence inside the spot compared to the others). The spots over the riblets and fins do appear to be somewhat elongated in the streamwise direction, and also appear to have grown slightly less in the spanwise direction.

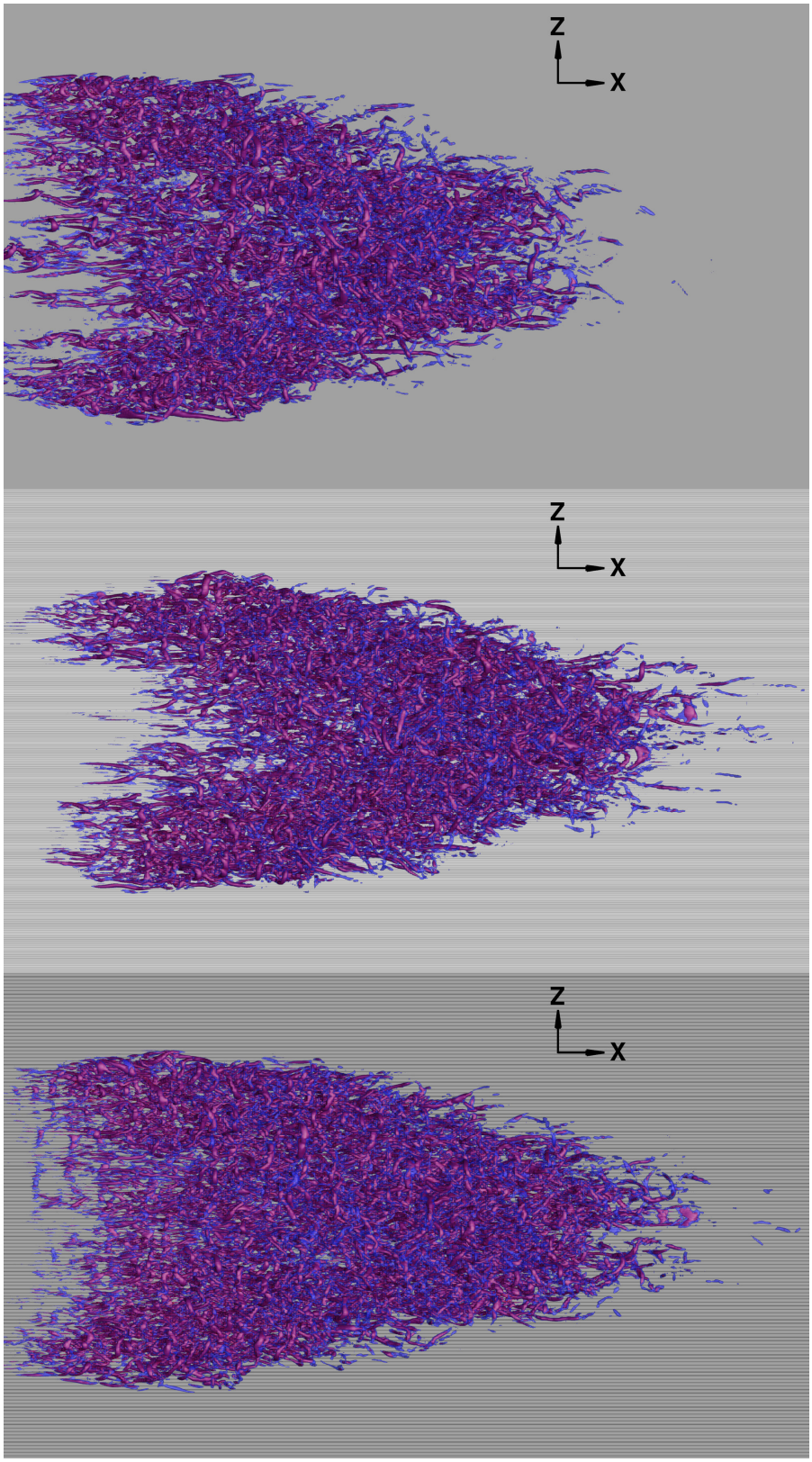

Figure 11: Close-up views of turbulent spots over a flat wall, riblets, and fins (from top to bottom). Spots are drawn with the same isosurfaces used in Fig. 8, and shown at t = 740.4 δ_o^*/U_∞.

Average Spreading Rate

As discussed previously, there are several ways to define the boundaries of a turbulent spot. Most often, the spot boundaries are defined by a cutoff value for some specific flow quantity. If the quantity is greater than the cutoff value in a specific region, then that region is defined to be part of the spot, otherwise it is considered outside the spot. Since one of the primary goals of this work is to investigate how the spreading of a spot is affected by surface textures, a consistent and precise definition of the spot edge or boundary is important. Several factors influenced the decision on how to define the spot. First, the chosen quantity should be near zero in a laminar, flat plate boundary layer. Even when textures are introduced, in the laminar case the quantity should be small throughout the majority of the domain. At the same time, it should become quite large (relative to the laminar case) inside the spot, so that it is useful for picking out the spot from the background flow. This is especially important in the presence of surface textures, since many quantities that could normally be used to define the spot (such as enstrophy, vertical velocity magnitude, and the magnitude of the vertical component of vorticity) become large not only inside the spot, but also along the crests of the textures and in the region where the textures begin. When examining multiple spots, at multiple time steps, it is not feasible to accurately "eyeball" the output to determine the edge of the spot. It is necessary to determine spreading angle in an automated way. Thus, it is essential that the chosen quantity picks out the spot from the textures without the need for qualitative examination in every case. The above considerations resulted in the choice of the magnitude of the streamwise component of vorticity, $|\omega_x|$, as the quantity which will define the spot.

During each time step the location of the "right" and "left" lateral edges of the spot are determined. Right and left are from the perspective of an observer looking downstream. The spot edge (for either the right or left side) is defined as the point on the spot which is farthest from the spot centerline (a straight line which is drawn from the centroid of the perturbation, parallel to the freestream direction). The spot edge on each side is calculated with three different cutoff values of $|\omega_x|$. These three values are averaged to give one location for the spot edge on each side. The cutoff values for $|\omega_x|$ are 0.188 U_∞/δ_o^*, 0.236 U_∞/δ_o^*, and 0.283 U_∞/δ_o^*.

At every time step, the final spot edge location is the average of 6 values (the right edge location defined with the three cutoff values of $|\omega_x|$, and the left edge defined with the same three cutoff values). Note that average values are computed for both the distance from the centerline to the spanwise edge of the spot (the spot half-width), and for the streamwise location of the spot edge. Once the spanwise edge location is averaged across the centerline, it is more accurate to refer to it as the spot half-width. Figure 12 shows a plot of the spot half-width vs. streamwise location of the spot edge for the flat wall, riblet, and fin cases.

In past work, we have focused on the spreading angle as the most useful measure of spot growth. However, due to the least squares regression used in the calculation (see Strand[6]), the spreading angle can be highly susceptible to discontinuous jumps in the streamwise location of the spot edge. These discontinuities occur frequently as new vortical structures first meet the cutoff value and are counted as part of the spot, and several of them can be seen in Fig. 12. This same problem was encountered by Singer[5]. Thus, we have decided to use the average spreading rate (the average time rate of change of the spanwise extent of the spot) as opposed to the spreading angle. These measures are closely linked, since it is well established in the literature that the spot moves downstream at a nearly constant speed. Our own work confirms this as well. Figure 13 is a plot of the streamwise location of the spot wingtip (relative to the initial perturbation) vs. time step for the flat wall spot once it has reached a fully-developed state. The data are clearly well fit by a straight line, and this is confirmed by the high R^2 value for a linear trendline which is least-squares fit to the data. Similar plots for the riblet and fin cases show the same linear relationship between wingtip location and time, thus indicating that in all three cases the wingtip is moving downstream at a nearly constant speed. With this in mind, we are confident in using the average spreading rate as a substitute for spreading angle.

Figure 14 shows a plot of the spot half-width vs. simulation time for the flat wall, riblet, and fin cases. We are interested in the average spreading rate of the fully-developed turbulent spot, so we are not concerned with the early growth of the vortical structures directly generated by the perturbation. Once this growth becomes self-similar, then the spot can be considered fully-developed. The spot can be considered fully-developed once the spot half-width becomes approximately linear as a function of time (with noise on top of the linear function, since spot growth is a chaotic process). Examining Fig. 14, this occurs around $t = 350\ \delta_o^*/U_\infty$, varying somewhat between the three cases.

We can now calculate an average spreading rate for the fully-developed spot in each case. For this average spreading rate, we use $t = 286.6\ \delta_o^*/U_\infty$ as our initial time, and $t = 859.8\ \delta_o^*/U_\infty$ as our final time (this is the time at which the simulation ended, and by this point the front tip of the spot had reached the end of the streamwise domain).

These average spreading rates are listed in Table 1 for all three cases. The percent differences between the texture cases and the flat wall case are also listed. When examining the difference in average spreading rate for the

developed spot, the riblets and fins are very similar in effect. Both reduce the average spreading rate by 7-8%. This is roughly in line with our previous results for the riblet case, but the current fin case shows only about half the reduction of the equivalent fin case from Strand[6]. That work used the spreading angle rather than the average spreading rate, however. In order to confirm that the textures are also decreasing the spreading angle, we also calculated the spreading angle for these spots, using a least-squares trendline as in Strand[6]. These spreading angles are shown for each spot in Table 2. As one final check, we also calculated another, simpler version of the spreading angle for each spot. This version only uses the flowfield from the last time step. The spot is defined as above, and the spreading angle is simply the angle shown in Fig. 1. This angle is calculated by dividing the spot half-width by the streamwise location of the spot wingtip (relative to the initial perturbation), and then taking the arctangent of this quantity. Spreading angles calculated in this way for each spot are shown in Table 3.

From Tables 1-3, it is clear that no matter how the spot spreading is quantified, this spreading is being reduced to some degree by the surface textures.

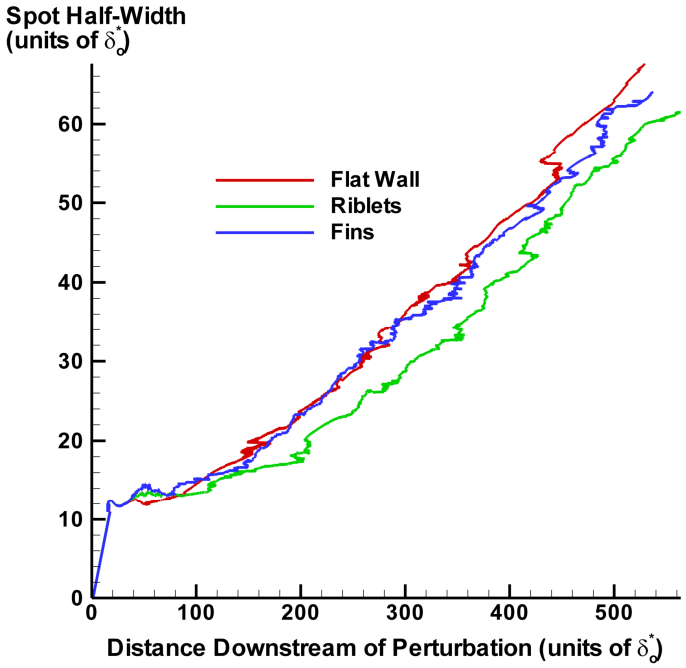

Figure 12: Spot half-width vs. streamwise location of the spot edge for the flat wall, riblet, and fin cases.

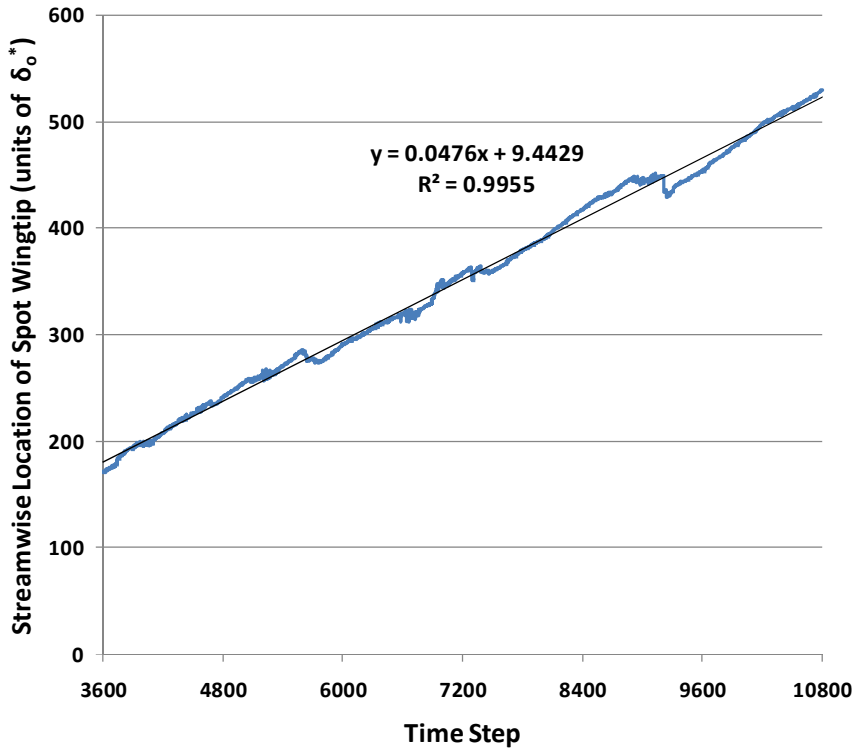

Figure 13: Streamwise location of the spot wingtip vs. time step for the flat wall spot once it has reached a fully-developed state. Linear least-squares trendline is shown as well. Note the high R^2 value, indicating that a straight line is a good fit to the data.

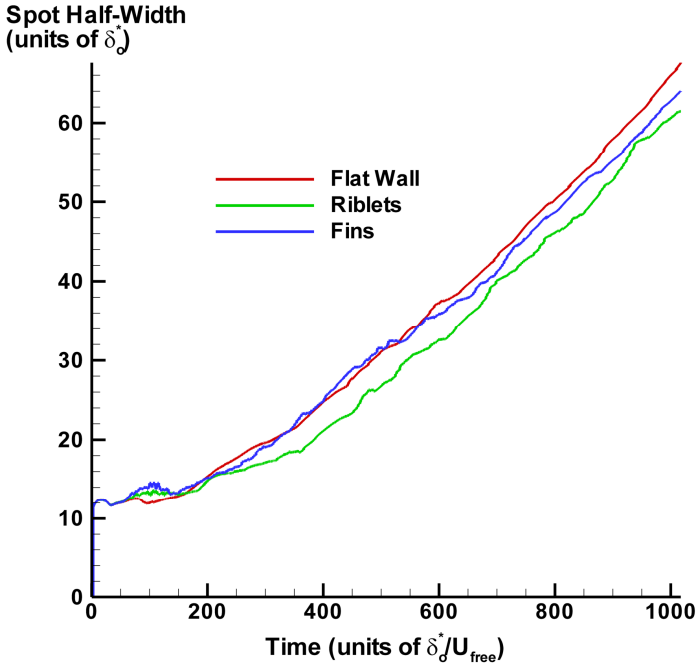

Figure 14: Spot half-width vs. simulation time for the flat wall, riblet, and fin cases.

Table 1: Average spreading rates for spots over the flat wall, riblets, and fins.

Texture Type	Average Spreading Rate (units of U_∞)	% Change Compared to Flat Wall
Flat Wall	**0.0812**	**-**
Riblets	**0.0753**	**-7.3**
Fins	**0.0750**	**-7.7**

Table 2: Spreading angles (as defined in Strand[6]) for spots over the flat wall, riblets, and fins.

Texture Type	Spreading Angle (°)	% Change Compared to Flat Wall
Flat Wall	**7.6**	**-**
Riblets	**7.1**	**-6.0**
Fins	**6.9**	**-8.8**

Table 3: Spreading angles (the simple version mentioned above) for spots over the flat wall, riblets, and fins.

Texture Type	Spreading Angle (°)	% Change Compared to Flat Wall
Flat Wall	**7.3**	**-**
Riblets	**6.2**	**-14.5**
Fins	**6.8**	**-6.6**

Grid Convergence

Finally, a word should be said about grid convergence. It is very difficult to establish grid convergence for these types of simulations. The growth of a turbulent spot is a chaotic process, and thus the final detailed structure of the spot is highly sensitive to the initial perturbation and to the exact texture shapes. Even in the case of spots over a flat wall, tiny differences in the eddy structure between two similar spots will grow chaotically over time, and after the spots have propagated a modest distance downstream they will appear completely different at the finest scales.

As discussed previously, the body forces that create the immersed boundaries (flat plate, textures, perturbation, buffer zone, and suction wall) are applied at the grid nodes. Even if the grid resolution is more than adequate to model the flowfield, simulations with different resolutions will still have differences in the body force field which is applied to generate the textures. Thus, even with vast computational resources, it would be nearly impossible to demonstrate grid convergence by comparing the exact eddy structure within spots simulated with different grid resolutions. Instead, the demonstration of grid convergence would require ensemble averaging. If the grid is converged, the ensemble averaged spot flowfield should be nearly identical after the grid resolution is increased. Unfortunately, practical computational time limits have prevented the use of ensemble averaging for grid convergence testing; each spot simulated herein took 36 days to run on 16 processors.

In order to study grid convergence in a more quantitative way, it is necessary to define a quantity of interest (QoI) so that we may examine grid convergence with respect to this specific quantity, rather than in a general, qualitative sense. The quantity of interest which is relevant to this work is the average spreading rate of a turbulent spot. With this QoI in mind, a grid convergence study was undertaken.

Previous work (Strand[6], and more recent work awaiting publication) has given us confidence that the grid is well resolved in the streamwise and spanwise directions, so the grid convergence study herein was limited to the wall-normal direction. Memory constraints prevented us from significantly increasing the grid in the wall-normal direction, so instead the grid resolution was cut in half and an additional flat wall case was run. The lower resolution is equivalent to that used in Strand[6], and at that time it was believed to be sufficient. Figure 15 shows a plot of spot half-width vs. simulation time for the original flat wall case and the lower wall-normal resolution flat wall case.

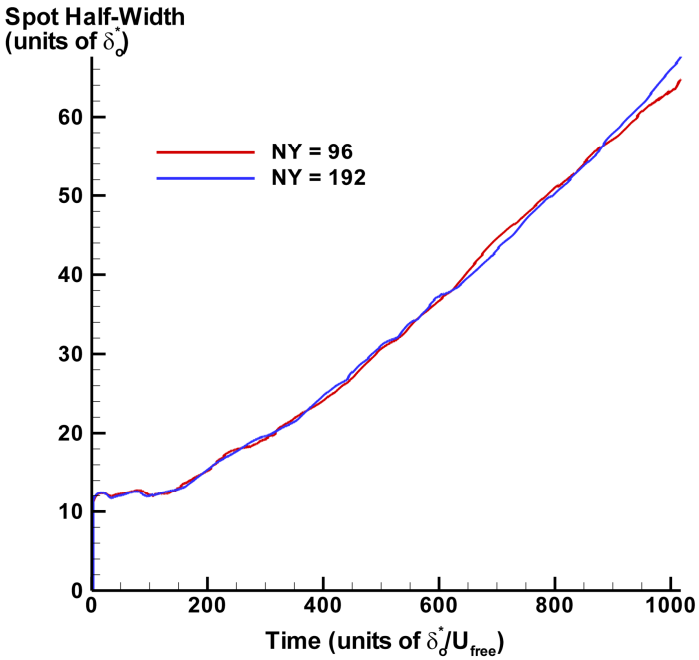

Figure 15: Spot half-width vs. simulation time for the original and lower wall-normal resolution flat wall cases.

It is apparent from Fig. 15 that the spot half-width is very similar in both cases for the majority of the simulation. This level of agreement is impressive considering the chaotic nature of the spot growth process. Based on the agreement seen in Fig. 15, we consider the full-resolution (NY = 192) case to be grid converged for our purposes.

IV. Conclusions and Future Work

Several conclusions can be drawn from the work presented here. First, it appears that turbulent spots are composed primarily of a multitude of interwoven hairpin vortices. In young spots these hairpins are all of a roughly similar size, while in more mature spots the range of hairpin scales increases greatly.

In prior work, passive surface textures such as riblets and fins have shown some promise in constraining spot spreading. This work has shown that textures can continue to effect the growth of more mature spots, which are at higher values of Re_x and have been followed significantly further downstream from the perturbation. Both of the surface textures examined herein decreased the average spreading rate of the spot by 7-8% when compared to the flat wall value.

These results are encouraging, because these textures still have not been fully optimized. The dimensions used for the textures were those of the riblets and fins that were most effective at constraining spot growth in previous work, but it is likely that the height and/or spacing of optimum textures will be a function of streamwise location along the plate. Further study could be performed with textures whose dimensions vary with streamwise distance. Other shapes could also be tried, such as cusped or sawtooth riblets.

Finally, it is useful to examine *why* the textures are able to constrain spot spreading. Better understanding of how the textures interact with the spot could allow for improved textures shapes and dimensions that could better constrain spot growth. This is the subject of current work by Chu et al.[12], also presented at this conference.

Acknowledgments

We would like to thank AFOSR for support through grant FA 9550-08-1-0453. We would also like to thank the Texas Advanced Computing Center (TACC) for the use of their computer resources.

References

[1]J. Wygnanski, M. Sokolov and D. Friedman, "On a Turbulent 'Spot' in a Laminar Boundary Layer," *J. Fluid Mechanics*, Vol. 78, 1976, pp. 785-819.

[2]J. Amini and G. Lespinard, "Experimental Study of an 'Insipient Spot' in a Transitional Boundary Layer," *Physics of Fluids*, Vol. 25, No. 10, Oct. 1982, pp. 1743-1750.

[3]D. Henningson, P. Spalart, and J. Kim, "Numerical Simulations of Turbulent Spots in Plane Poiseuille and Boundary Layer Flow," *Physics of Fluids,* Vol. 30, No. 10, Oct. 1987, pp. 2914-2917.

[4]B. Singer and R. Joslin, "Metamorphosis of a Hairpin Vortex into a Young Turbulent Spot," *Physics of Fluids*, Vol. 6, No. 11, Nov. 1994, pp. 3724-3736.

[5]B. Singer, "Characteristics of a Young Turbulent Spot," *Physics of Fluids*, Vol. 8, No. 2, Feb. 1996, pp. 509-521.

[6]J. S. Strand, "DNS of Surface Textures to Control the Growth of Turbulent Spots", Master's Thesis, The University of Texas at Austin, December 2007.

[7]D. B. Goldstein, R. Handler, and L. Sirovich, "Modeling a No-Slip Flow Boundary with an External Force Field," *J. Comp. Phys*., Vol. 105, 1993, pp. 354-366.

[8]R. A. Handler, E. W. Hendricks, and R. I. Leighton, "Low Reynolds Number Calculation of Turbulent Channel Flow: A General Discussion," NRL Memorandum Report 6410, 1989, pp. 1-103.

[9]J. Kim, P. Moin, and R. Moser, "Turbulence Statistics in Fully Developed Channel Flow at Low Reynolds Number," *J. Fluid Mechanics*, Vol. 177, 1987, pp. 133-166.

[10]D. Goldstein, J. Cohen and V. Levinski, "DNS of Hairpin Vortex Formation in Poiseuille Flow Due to Two-hole Suction," Presented at 3rd AFOSR Int. Conf. on DNS and LES, Arlington, TX, Aug. 2001.

[11]J. S. Strand and D. Goldstein, "DNS of Surface Textures to Control the Growth of Turbulent Spots", AIAA 2007-1312, 45th AIAA Aerospace Sciences Meeting and Exhibit, 8 - 11 January 2007, Reno, Nevada.

[12]J. Chu, J. Strand, and D. Goldstein, "Investigation of Turbulent Spot Spreading Mechanism," AIAA-2010-0716, 48th AIAA Aerospace Sciences Meeting, 4-7 January 2010, Orlando, Florida.

[13]A. Jocksch and L. Kleiser, "Growth of Turbulent Spots in High-Speed Boundary Layers on a Flat Plate," *International Journal of Heat and Fluid Flow*, Vol. 29, 2008, pp. 1543-1557.